UNIVERSITY OF LEEDS

This is a repository copy of *Effect of cooling rate on the microstructure of rapidly solidified SiGe*.

White Rose Research Online URL for this paper:
http://eprints.whiterose.ac.uk/148449/

Version: Accepted Version

Article:
Hussain, N, Mullis, AM orcid.org/0000-0002-5215-9959 and Haque, N (2019) Effect of cooling rate on the microstructure of rapidly solidified SiGe. Materials Characterization, 154. pp. 377-385. ISSN 1044-5803

https://doi.org/10.1016/j.matchar.2019.06.014

© 2019, Elsevier. This manuscript version is made available under the CC-BY-NC-ND 4.0 license http://creativecommons.org/licenses/by-nc-nd/4.0/.

Reuse
This article is distributed under the terms of the Creative Commons Attribution-NonCommercial-NoDerivs (CC BY-NC-ND) licence. This licence only allows you to download this work and share it with others as long as you credit the authors, but you can't change the article in any way or use it commercially. More information and the full terms of the licence here: https://creativecommons.org/licenses/

Takedown
If you consider content in White Rose Research Online to be in breach of UK law, please notify us by emailing eprints@whiterose.ac.uk including the URL of the record and the reason for the withdrawal request.

White Rose university consortium
Universities of Leeds, Sheffield & York

eprints@whiterose.ac.uk
https://eprints.whiterose.ac.uk/

Effect of Cooling Rate on the Microstructure of Rapidly Solidified SiGe

Naveed Hussain[a], Andrew M Mullis[a], Nafisul Haque[ab]

[a]School of Chemical & Process Engineering, University of Leeds, Leeds LS2 9JT, UK.

[b] Department of Metallurgical Engineering, NEDUET, University Road, Karachi 75270, Pakistan.

Abstract

Si-30 wt% Ge (14.2 at.% Ge) alloy has been subject to rapid solidification by drop-tube processing, with the resulting powders being subject to cooling rates between 1800 and 20000 K s^{-1}. Microstructure characterisation was conducted via SEM which showed the formation of distinctive Si-rich grains with Ge localised at the grain boundaries in what appeared to be small discrete crystallites. EDX was used to determine the Ge concentration at the grain boundaries wherein contrary to expectation it was found that partitioning increased with increasing cooling rate. EDX performed in the TEM revealed that the Ge-rich regions at the grain boundaries had compound like preferred compositions, with Ge:Si ratios of 3:2 and 7:1 being observed, neither of which would be expected from the phase diagram. However, EBSD and TEM diffraction analysis show that these Ge-rich regions are not distinct compounds, having the same crystal structure and orientation as the Si-rich grain to which they are attached. There is also no evidence for chemical ordering. As such, the origin of these compound like regions of preferred composition remains enigmatic.

Keywords: Solidification microstructures; rapid solidification; semiconductor compounds; thermoelectric alloys.

1.0 Introduction

Tuneable band gap semiconductor materials, such as $Si_{1-x}Ge_x$ alloy, have recently attracted much attention as they offer greater flexibility than pure silicon for microelectronic applications [1]. Si-Ge alloys are known to exhibit high mechanical strength, a high melting point and low thermal conductivity at high temperatures (900 to 1200 K) [2]. This suite of properties makes Si-Ge alloys ideal materials for thermoelectrical power generation at temperatures around 1300 K, with applications ranging from power sources for artificial satellites to recovery of waste heat during industrial processing. Si-Ge alloys have been of particular interest as a means of power recovery in the steel industry during processing of steel billet and strip as it comes off the mill, with the operating temperature of Si-Ge thermoelectric generators being well matched to the hot working temperature of strip steel.

The basis of all thermoelectric power generation is that a suitable material can convert a temperature difference into a potential difference. The efficiency of electrical generation using heat applied to a thermoelectric material is defined by the dimensionless figure of merit:

$$ZT = \sigma S^2 T / \kappa$$

where σ is the electrical conductivity, S is the Seebeck coefficient, T the absolute temperature and κ is the thermal conductivity. The actual efficiency of generation, η_{max}, is then given by the product of a reduction factor along with the Carnot efficiency $(T_h - T_c)/T_h$:

$$\eta_{max} = \frac{T_h - T_c}{T_h}\left[\frac{\sqrt{1 - ZT_{ave}} - 1}{\sqrt{1 - ZT_{ave}} + T_c/T_h}\right]$$

where T_h and T_c are the hot- and cold-side temperatures, respectively, and ZT_{ave} is the figure of merit evaluated at $T_{ave} = (T_h + T_c)/2$. Conversely, the power generation capacity per unit volume of material is determined by the power factor:

$$Power\ Factor = \sigma S^2$$

Ideally, a good thermoelectric material should combine a high power factor and a high figure of merit, although in space confined applications a high power factor may be more important.

For optimal thermoelectric performance the composition of the Si-Ge alloy should be homogeneous at both the micro- and macro-scale, with any compositional variation altering the band gap and hence the performance. However, it should be noted that the melting points of Si and Ge are significantly different [3], and it is clear from the phase diagram there is a large separation between the solidus and liquidus line. Consequently, during crystallisation Ge, which has the lower melting point, is rejected from growing crystallites and concentrates in the residual liquid. This leads in turn to the formation of Si-rich grains surrounded by Ge-rich grain boundaries. Moreover, as is the density of molten elemental Si and Ge [4] are very different this can result in macro-segregation, wherein compositional gradients can exist across the resulting ingot.

$Si_{80}Ge_{20}$ alloys have previously been used for deep space satellite missions in radioactive isotope generators due to their suitability in converting energy from high temperature heat sources to electrical energy. $Si_{85}Ge_{15}$ P1 n-type material is used commercially in conjunction with a manganese silicide p-type material in thermoelectric generators that are suited to recover waste heat in processes at high temperature. The relatively high Ge content material is used due to the high thermal conductivity of Si-Ge materials with lower Ge content. However, the challenge in industry is to increase cost-efficiency by moving to Ge-lean compositions without affecting the thermoelectric characteristics of the resulting Si-Ge alloys, the US Geological Survey reporting 2017 year-mean prices for Ge as being more than ten times that of Si (1358 USD/kg for Ge metal compared to 110 USD/kg for Si metal). Using a nanostructuring approach, Si-Ge alloys with compositions of $Si_{92}Ge_8$ [5] [6] and $Si_{95}Ge_5$ [7] have previously been developed, this representing a lower Ge content than any commercial Si-Ge alloy available.

Due to the known effects of grain refinement and reduced segregation produced by rapid solidification, a number of such studies have been undertaken on Si-Ge alloys. Electromagnetic levitation studies have found that the development of the microstructure is associated with the solidification conditions, so it is possible to decrease the thermal conductivity of Ge-lean compositions by departing from thermodynamic equilibrium [8] [9] [10]. In a previous study by Zhang et al. n-type Si-Ge samples were synthesised using melt spinning and compared against slow cooled Si-Ge samples of the same composition. SEM and EDS were employed to analyse the samples, with it being found that during slow solidification the microstructure appeared inhomogeneous. In contrast, the microstructure of the rapidly solidified samples displayed greater homogeneity with less segregation, which was attributed to solute trapping. In relation to the cooling rate Zhang et al. also found that the grain size decreased with an increasing cooling rate [11].

Another study in 2002 compared Si-Ge samples processed in microgravity using the Japan Microgravity Center's (JAMIC's) drop shaft and a 10m drop tube to equivalent samples processed under normal gravity conditions. It was found that the samples processed under terrestrial conditions displayed greater segregation in the microstructure, although segregation was not fully suppressed even in the samples processed in microgravity. It was thought that segregation occurred due to diffusion during unidirectional solidification [12]. Both studies found that the Si-rich regions were the first to solidify, with the Ge-rich regions forming towards the edges and boundaries of the large distinctive Si-rich grains.

A study by Panofen and Herlach [13] on Si-2.5 at.% Ge was conducted using electromagnetic levitation in order to understand the characteristics of growth. At low undercooling the first region of growth was determined to be planar faceted growth, while at higher undercooling the growth of faceted dendrites was determined. It was also observed that a higher concentration of Ge existed at the centre of the droplets. Given that partitioning results in a Ge-rich residual liquid it was inferred that growth

proceeded from the surface to the centre. In 2018 Herlach et al. [14] conducted electromagnetic levitation on a further range of Si-Ge compositions: $Ge_{25}Si_{75}$, $Ge_{50}Si_{50}$, and $Ge_{75}Si_{25}$, with similar growth kinetics being found. The critical undercooling for the transitions from faceted to dendritic and dendritic to planar growth was determined in each case. For all compositions the transition undercooling was found to be in the range 200-230 K, with slightly higher undercoolings being observed in the dilute alloys at both the Si-rich and Ge-rich ends and the lowest undercooling being found for the equimolar composition.

2.0 Experimental procedure

Pre-alloyed Si–30 wt% Ge (Si–14.2 at.% Ge) was obtained from Goodfellow in lump form, these being pieces of broken, directionally solidified ingot. The starting material was characterised using Scanning Electron Microscopy (SEM) and powder X-Ray Diffraction (XRD).

For rapid solidification processing a 6.5 m high-vacuum drop tube was used. Small pieces of ingot, with a total mass of around 4 g, were loaded into an alumina crucible which contained three × 300 μm laser drilled holes in the base. The crucible was mounted inside a graphite susceptor which makes a pressure tight seal to a flange at the top of the drop-tube, allowing the crucible to be pressurised in order to eject the alloy once molten. The crucible and susceptor, together with a twin-walled alumina heat-shield sit inside an induction coil at the top of the drop-tube which is connected to a 3 kW RF generator. The arrangement is shown schematically in **Figure 1**.

Prior to melting, the tube is evacuated to a pressure of 1 Pa using a two-stage, oil-filled rotary pump and then flushed with oxygen free nitrogen at a pressure of 40 kPa, this procedure being repeated 3 times. The tube is then evacuated to a pressure of 10^{-4} Pa using a turbomolecular pump before again being filled to 40 kPa with oxygen free nitrogen gas. This procedure ensures that an oxygen and water free environment is obtained into which the molten alloy is sprayed. To determine the temperature within the melt crucible an R-type thermocouple was used. An estimated 50 K superheat was achieved

during a 95-minute heating cycle before the melt was ejected from the crucible by pressurising it with 400 kPa of nitrogen gas. Further details of the drop-tube method can be found in Ref. [15].

After the solidified droplets were collected they were sieved into the following standard sieve sizes: 850 μm < d, 500 μm < d < 850 μm, 300 μm < d < 500 μm, 212 μm < d < 300 μm and 150 μm < d < 212 μm, with d being the particle diameter. The method in Ref. [15] was used to estimate the cooling rates of free-falling particles from the balance of heat fluxes. The estimated cooling rates for the undercooled liquid of the following particles sizes: 150, 212, 300, 500 and 850 μm, were 20000, 12000, 7200, 3600 and 1800 K s^{-1} respectively.

During ejection, and pressurisation of the crucible, some of the Si-Ge melt remained in the crucible, which is thought to have occurred due to the crucible base not being perfectly flat. EDX analysis (described below) was used to confirmed that the residue, starting material and drop-tube particles were all of the same composition.

Samples were prepared for Scanning electron microscopy (SEM) by mounting in TransOptic™ resin. Samples were then ground and polished using 5, 3 and 1 μm diamond paste before being attached to an SEM stub. Finally, the sample was sputter coated using a layer or carbon. Full details of sample preparation for SEM analysis can be found in Ref [16].

Microstructural analysis was performed using a Hitachi SU8230 SEM in backscattered detection mode, wherein images are obtained in atomic number (Z) contrast. Due to the large difference in Z between Si and Ge this gives good contrast between the Si-rich grains and the Ge-rich grain boundary region. In order to obtain high spatial resolution images a low accelerating voltage ($V_{\mathrm{acc}} = 5$ kV) was utilised, so minimising the backscatter interaction volume. The probe current (I_{e}) was 30 μA. The grain size distribution contained within the resulting micrographs was analysed using ImageJ software [17]. Electron Dispersive X-Ray (EDX) Spectroscopy maps were obtained for each sieved sample sizes with EDX point measurements and EDX line-scans also taken in regions of interest within the micrographs.

The starting Si-Ge ingot and the residual material left in the crucible during the drop tube experiment was also subject to EDX line-scan and point measurements.

In order to prepare samples for Transmission Electron Microscopy (TEM) the samples were milled using a FEI Helios G4 FEGSEM focused ion beam. Precision milling was conducted using a high energy Ga+ beam, with the area of interest from the sample being welded onto a TEM grid. The sample was then sliced to < 100 nm in thickness using the ion beam. TEM brightfield images and selected area diffraction patterns were acquired for rapidly solidified Si-Ge samples using an FEI Titan Themis TEM operating at 300kV. Images were obtained using the Gatan OneView 16-megapixel CMOS digital camera. The Super-X EDX system was also fitted with a windowless 4 detector design, allowing for EDX mapping and EDX line-scans to be conducted using the Velox 2.4 software.

The importance of sample preparation is heightened when preparing for EBSD. Following the sample preparation process previously mentioned one sample, 850 – 500 μm, was further polished for 10 minutes using 0.1 μm colloidal silica suspension on a Buehler Automet 250 grinder-polisher machine. The polishing settings used were: Force = 25 N, speed of base = 130 rpm and speed of head = 50 rpm. Grain orientation maps were obtained using an FEI Quanta 650 FEGSEM with Oxford/HKL Nordlys EBSD system.

3.0 Results

3.1 CALPHAD Modelling

The calculated Si-Ge phase diagram is shown in **Figure 2**. Si-Ge is a particularly simple system displaying a continuous solid solution over the whole compositional range. For a melt at a composition of 30 wt% Ge (14.2 at.% Ge) the first solid to form will have a composition of 14.0 wt% Ge, giving a partition coefficient, k_E, of 0.47. The predicted evolution of the solid fraction with temperature, assuming ideal Scheil conditions, is shown in the left-hand axis of **Figure 3**. Upon cooling below the

liquidus temperature the solid fraction is predicted to initially increase relatively quickly at approx. 0.01955 K^{-1}, with this value dropping to 0.0005 K^{-1} by 0.85 solid fraction. The corresponding instantaneous composition of the solid growing at that temperature is shown on the right hand axis of **Figure 3**. The composition of the solid initially changes relatively slowly with increasing solid fraction, with the composition of the solid not reaching the starting composition of 30 wt% Ge until a solid fraction of 0.57 is attained. However, thereafter the Ge concentration of remaining solid increases rapidly reaching 59.4 wt% Ge at a solid fraction of 0.90 and finally approaching 100% Ge at the end of solidification.

3.2 SEM Microstructure Characterisation

A section of the starting ingot was analysed using SEM backscatter to compare with rapidly solidified samples. The SEM micrograph, seen in **Figure 4**, appears to display a heterogeneous microstructure with several regions of varied Ge concentration. There is also a clearly visible directionality, which is as to be expected in a chill-cast ingot.

The microstructure of the crucible residue, also as determined by SEM backscatter, is displayed in **Figure 5**. A heterogeneous microstructure can also be observed in the residual sample but with no obvious directionality. Si-rich regions appear to dominate the majority of the visible area with smaller Ge-rich regions clustered together at the margins of the larger Si-rich regions. Fairly extensive partitioning is evident in both samples. Point EDX measurements have been made at a number of locations in each micrograph with a view to determining the maximum and minimum Si and Ge concentrations within the field of view. The maximum Si concentration is consistent across both micrographs at 83-84 wt% Si, which is also in good agreement with the Scheil calculation. The maximum Ge concentrations observed were 73.1 wt% in the starting material and 52.5 wt% in the crucible residue. We note that both are well below the almost pure Ge predicted by the Scheil calculation for the last material to solidify.

Figures 6A – 6E show the typical SEM backscatter micrographs for each size fractions obtained by sieving of the drop tube powders. The microstructure of all five samples is broadly similar, comprising relatively large, Si-rich grains with extensive Ge localising at the grain boundaries. It is also apparent that the Si-rich grains decrease markedly in size as the cooling rate increases. This shall be quantified below. Also visible are several 'cross' shapes located close to the centre of some of the Si-rich grains, possibly a result of coring. These cores, which are remnants of the initial of dendrite formation, is consistent with the expected partitioning behaviour in the Si-Ge system.

EDX area scans have been conducted over the whole field of the micrographs presented in **Figures 6A – 6E**, these confirming that the bulk composition of the samples is equal to the composition of the starting material to within ± 2 wt%, which is comparable with the experimental error expected for EDX composition measurement. As with the starting material and crucible residue, point EDX measurements have been made to establish typical values for the maximum and minimum Si and Ge concentrations in each sample. The results of these measurements are shown directly on the figure, with circles indicating the location of the measurements. The composition measurements are also summarised, as a function of cooling rate, in **Figure 6f**. The minimum Ge concentration shows a consistent pattern across samples, with a value around 15 wt%, which as above is in good agreement with the Scheil calculation. In contrast, the maximum Ge concentration at the grain boundaries appears to increase systematically with increasing cooling rate from a value of 71.1 wt% for the 850 μm sample ($\dot{R}$ = 1800 K s^{-1}) to 98.3 wt% for the 150 μm sample ($\dot{R}$ = 20000 K s^{-1}).

The grain size distribution for the 5 drop tube processed samples, together with the crucible residue, has been measured using ImageJ, with each measurement being made across several micrographs from each sample. **Figure 7** shows the mean area of the Si-rich grains as a function of cooling rate. Cooling rates for the five drop-tube samples are estimated from the balance of heat fluxes, as described above. For the crucible residue the cooling rate was measured directly from the

temperature-time history of the furnace, wherein $\dot{R}$ = 10 K min^{-1} = 0.33 K s^{-1}, meaning that the results cover close to 5 orders of magnitude in cooling rate. Error bars are based upon the standard deviation of the measured grain sizes and consequently are representative of the degree of variability observed in the grain size distribution. As might be expected the mean area per grain is observed to decrease with increasing cooling rate, with the mean area dropping by almost exactly one order of magnitude from 3200 μm^2 in the crucible residue to 320 μm^2 in the smallest drop-tube sample.

Upon detailed examination of the Ge-rich regions it appears that the Ge-rich regions appear to form as independent crystallites which decorate the boundaries of large, Si-rich grains. This is illustrated in **Figure 8** which shows a region from a sample in the 500 – 300 μm sieve fraction. In addition, it is noticeable that the transition from the Si-rich to Ge-rich region is quite abrupt, with in places a seemingly discontinuous change in the grey level. This type of discontinuous change in contrast is common when observing stoichiometric compounds but would not be expected in a continuous solid solution. To obtain a better understanding of the grain boundary region TEM analysis has been conducted, while EBSD analysis has been conducted to determine whether the Ge-rich regions are separate crystallites, and if so their orientation relationship with the large Si-rich grains.

3.3 SEM and TEM EDX Line-scan Analysis

Drop tube processed samples were subject to TEM analysis, including EDX, due to the compound-like appearance of the Ge-rich regions in the SEM backscatter micrographs. **Figure 9A** shows a TEM bright-field image obtained from the grain boundary region of a sample in 850 – 500 μm sieve size. As with the SEM micrographs, there are a number of clear step changes in the contrast displayed within the microstructure. To the left-hand side of the micrograph is the boundary of one of the large Si-rich grains, with the transition into the Ge-rich grain boundary delineated by a clear change in contrast. A further contrast step change may be observed towards the right-hand margin of the micrograph. In order to establish the composition of these regions, TEM-EDX analysis has been conducted. **Figure**

9B shows the results of one such EDX line-scan, obtained from the window depicted in **Figure 9A** which, as can be seen, spans the three main areas of differing contrast in the micrograph. It is immediately apparent from the EDX results that each of the three regions within the micrograph have very distinct compositions, with a step-change in the composition at the boundaries.

The left-hand region, some 0.7 μm wide, corresponding to the margin of a large Si-rich grain, has a composition around 30 at.% Ge. SEM-EDX, discussed below, suggest that the large Si-rich grains display a continuously varying composition in close agreement with the Scheil calculation and for this reason we believe that the apparent constant composition displayed in the TEM-EDX scan may be an artefact of the relatively small area sampled. At 0.7 μm there is a step-change in Ge content to 60 at.%, with the composition then being constant until 2.7 μm when there is a second step-change to a composition of 86-87 at.% Ge. These two region at 60 and 86-87 at.% Ge, with their uniform compositions that follow simple integer ratios (Ge:Si of 3:2 and possibly 7:1 for a composition of Si-87.5 at.% Ge) are far more reminiscent of stoichiometric compound formation at the grain boundary, rather than the continuous increase in Ge that would be expected from two elements which display a continuous solid solution over their whole composition range. This presumably is what gives the appearance in the backscatter micrographs of the boundaries of the large Si-rich grains being decorated with much smaller Ge-rich grains.

In order to establish whether there is a similar tendency for preferred stoichiometry in the Si-rich regions, SEM-EDX has been employed, where we trade off the lower spatial resolution of the SEM for the ability to sample much larger areas characteristic of whole grains. **Figure 10** shows one such EDX trace across an Si-rich grain. The minimum Ge concentration is around 6 at.% (14-15 wt%) which is consistent with both the spot measurements shown in **Figure 6** and the Scheil calculation. Moreover, the composition appears to increase continuously moving towards the Ge-rich grain boundary region,

with no indication of any preferred compositions. Consequently, it appears that the formation of these regions of preferred composition is confined to the Ge-rich grain boundaries.

3.4 Electron Backscatter Diffraction

SEM and TEM EDX results indicate that the growth characteristics of rapidly solidified Si-Ge do not follow the Scheil solidification sequence towards the end of solidification, with the apparent formation of smaller Ge-rich grains at the boundaries of the large Si-rich grains. Moreover, these small Ge-rich grains appear to have discrete compositions more redolent of compound formation. In order to determine whether these apparent Ge-rich grains are true grains, i.e. that they have crystallographically distinct orientations from the Si-rich grains they boarder, EBSD analysis has been undertaken. **Figure 11A** shows the grain orientation mismatch, or Euler map, for a sample in the 850-500 μm sieve sample, with for reference, a backscatter image of the identical field of view shown in **Figure 11B**. The large grains in the Euler map seem to correspond well to the Si-rich grains in the backscatter image but, more importantly, the apparent Ge-rich grains do not show up on the Euler map, indicating that they have the same crystallography as, and are epitaxial with, the larger Si-grains which they boarder. What is apparent by careful comparison of the two images comprising **Figure 11** is that the Ge-rich region can always be associated with just one Si-rich grain and that the grain boundary as determined by EBSD runs along the interface between the Ge-rich region and the neighbouring Si-rich grain. The arrows in **Figure 11** illustrate this. With reference to the arrow on the right-hand side of the micrograph we can see from the Euler map that the Ge-rich region belongs wholly to the grain to its left shaded blue. Similarly, with reference to the arrow on the left-hand side of the micrograph we can see that the Ge-rich region belongs wholly to the grain above it shaded purple. Moreover, there does not appear to be any preferred directionality in this. Analysis of a number of such images shows that the Ge-rich regions are equally likely to be associated with grains to their left or right and to with those above or below them.

3.5 Selected Area Diffraction Patterns

In light of the EBSD results TEM selected area diffraction (SAD) analysis was undertaken to determine any differences in the crystallography between the Ge-rich and Si-rich regions. TEM SAD was conducted on the three distinct regions seen in **Figure 9** and the results are given in **Figure 12**. **Figure 12A** shows the SAD pattern of the Ge-rich region, **Figure 12B** shows the SAD pattern of the intermediate region, and the Si-rich region SAD pattern can be found in **Figure 12C**. By observing the SAD patterns, it is apparent that all regions appear to have the same crystal structure: diamond cubic, and none of the regions appear chemically ordered, which is apparent due to the absence of superlattice spots. The lack of chemical ordering is expected with a solid solution but might have been expected given the stoichiometric nature of the Ge-rich regions.

4.0 Discussion

Si-Ge alloy, at the 30 wt% Ge composition commonly used as a commercial thermoelectric material, has been subject to rapid solidification processing using the drop-tube method, wherein estimated cooling rates between 1800 - 20000 K s^{-1} are encountered. A decrease in the average grain size is observed as the cooling rate is increased, with the average grain area decreasing from ≈ 850 μm^2 at the lowest cooling rate to 320 μm^2 at the highest cooling rate. This compares with a value of 3200 μm^2 for material cooled at the furnace cooling rate of 0.33 K s^{-1}. All of this is as expected and can be accounted for by standard solidification theory, namely that higher cooling rates are favouring enhanced nucleation over growth, which is likely to be sluggish given the faceted growth mode likely for Si-Ge.

However, what is also clear is that we observe a steady decrease in grain size, with no evidence for an abrupt drop such as would be observed in spontaneous grain refinement (SGR). This contrasts with the work of Herlach and co-workers [13] [14] who observed such grain refinement transitions in a range of Si-Ge alloys undercooled by electromagnetic levitation, with the transition being ascribed to a change in the crystal growth mode from faceted to dendritic. It is not clear whether the failure to

observe SGR in this study was due to insufficient undercooling being achieved or whether the high cooling rates experienced by our samples inhibited the transition. Based on the work of Panofen & Herlach [13] we estimate an undercooling of around ΔT = 200 K being required to initiate the SGR transition in our alloy. It is not possible to measure the nucleation temperature and hence undercooling of individual droplets, but the maximum undercooling can be estimated, for instance using the model of Wang & Wei [18], wherein values ranging from ΔT = 52 K for an 850 μm droplet to ΔT = 268 K for a 150 μm droplet are obtained. We might have expected therefore to see some spontaneously grain refined samples in our smallest sieve fraction and as we do not we are inclined to favour the idea that SGR is inhibited by rapid cooling. This would be consistent with observations in other systems. This is significant for commercial producers of Si-Ge thermoelectric alloys hoping to utilise SGR as a means of obtaining fine grained material, with most industrial rapid solidification processing being based upon rapid cooling techniques (melt spinning, atomisation) rather than deep undercooling.

We find that with increasing cooling rate solute partitioning becomes more extreme. Peak Si concentrations of around 85 wt% at the centres of the large, Si-rich grains are determined fairly consistently irrespective of cooling rate and in close agreement with a Scheil calculation for the solidification pathway. However, the peak Ge concentration at the grain boundary increases systematically with cooling rate from 71.1 wt% for the 850 μm sample ($\dot{R}$ = 1800 K s^{-1}) to 98.3 wt% for the 150 μm sample ($\dot{R}$ = 20000 K s^{-1}) and is only 52.5 wt% at the grain centres in the crucible residue ($\dot{R}$ = 0.33 K s^{-1}).

This result is somewhat paradoxical as the onset of solute trapping with increased cooling rate would normally be expected to supress partitioning, leading to a more homogeneous compositional distribution. We note that due to the reduction in grain size with increasing cooling rate this is unlikely to be an instrumental artefact. EDX measurements become more difficult as the characteristic length scale of the microstructure decreases, wherein the large interaction volume associated with high energy

electrons used to excite X-ray emissions may sample not only the region of interest but surrounding areas as well. However, in this case that would lead to a reduced Ge concentration being measured as the beam would sample increasingly large fractions of the surrounding Si-rich material as the grain size decreased.

From **Figure 6f** it is clear that the Ge concentration in the grain centres is almost independent of cooling rate. As this will represent the first material to solidify this implies that the partition constant at the start of solidification was close to its equilibrium value for all cooling rates studied here, i.e. none of these samples attained a growth velocity at which significant solute trapping occurred. However, for cooling rates < 5000 K s^{-1}, the Ge concentration at the grain boundaries, which represents the last material to solidify, increases with increasing cooling rate before plateauing for cooling rates < 5000 K s^{-1}. We also note that the measured Ge concentration for the higheer cooling rate is approaching that predicted by the Scheil calculation. This suggests that the less severe partitioning observed at lower cooling rate may be due to significant back diffusion during, or immediately after, solidification equalising the composition in the grain boundary region. As the cooling rate is increased there would then be less time for such back diffusion and the Scheil limit would be approached. This result is significant for the commercial processing of these alloys as it would normally be assumed that rapid solidification processing would lead to a more chemically homogeneous product. In fact, the contrary appears to be the case.

The observed microstructure of the rapidly solidified Si-Ge alloy consisted of large Si-rich grains with Ge concentrated at the grain boundaries. In backscatter imaging these Ge-rich regions have the appearance of small crystallites that decorate the boundaries of the large Si-rich grains. Interestingly, careful observation of previously published micrographs, e.g. Figure 3 in Zhang et al. [11], show identical features, although the original authors appear not to have commented upon these features. In fact, TEM and EBSD analysis reveal that these Ge-rich regions are generally part of one of the Si-rich grains to which they are attached, rather than being separate crystallites. Their appearance of being

discrete crystallites is produced by abrupt contrast changes brought about by a non-continuous Ge-distribution in the grain boundary region, which is perhaps the most unusual feature of the results presented here. Contrary to the accepted equilibrium phase diagram for Si-Ge, which shows a continuous solid solution over the whole composition range, we find that in the Ge-rich grain boundary regions there is evidence of compound like formations. By this we mean that we find extended regions of constant composition with step changes in composition between adjacent regions. Moreover, these discrete compositions correspond to simple integer ratios, with for instance a region at Si-60 at.% Ge which would correspond to Si_2Ge_3. However, although these regions have compound like compositions, both TEM-SAD and EBSD show that they are crystallographically identical to the Si-rich Si-Ge solid solution and indeed TEM-SAD analysis shows no evidence for chemical ordering as would typically be expected for a stoichiometric compound. Consequently, the origin of these compound like regions remains enigmatic. However, the formation of such regions may be significant for the performance of Si-Ge alloy as efficient thermoelectric materials, with the step-change in composition at the grain boundary leading to various effects such as increased scattering and localised heating. As such the understanding of these compound like regions is critical to the future development of these high temperature thermoelectric materials.

Acknowledgements

This work was supported by the Engineering and Physical Sciences Research Council Doctoral Training Partnership [ref. 1633900].

The authors thank the European Space Agency (ESA) for financial support within the NEQUISOL project, contract number 15236/02//NL/SH.

Data Availability

The raw/processed data required to reproduce these findings cannot be shared at this time due to technical or time limitations.

References

[1] R. R. King, N. H. Karam and M. Haddad, "Multijunction photovoltaic cells and panels using a silicon or silicon-germanium active substrate cell for space and terrestrial applications.". US Patent US 6340788 B1, 2002.

[2] C. B. Vining, "Thermoelectric Properties of Silicides," in CRC Handbook of Thermoelectrics, 1 ed., N. Sullivan, Ed., CRC Press LLC, 1995, pp. 329-337.

[3] R. W. Olesinski and G. J. Abbaschian, "The Ge-Si (Germanium-Silicon) System," Bulletin of Alloy Phase Diagrams, vol. 5, no. 2, pp. 180-183, 1984.

[4] W.-K. Rhim and T. Ishikawa, "Thermophysical Properties of Molten Germanium Measured by a High-Temperature Electrostatic Levitator," International Journal of Thermophysics, vol. 21, no. 2, pp. 429-443, 2000.

[5] G. Bernard-Granger, K. Favier, M. Soulier, C. Navone, M. Boidot, B. Deniau, P. Grondin, J. Leforestier and J. Simon, "Thermoelectric properties of an N-type silicon–germanium alloy related to the presence of silica nodules dispersed in the microstructure.," Scripta Materialia, vol. 93, p. 40–43, 2014.

[6] G. H. Zhu, H. Lee, Y. C. Lan, X. W. Wang, G. Joshi, Z. W. Wang, J. Yang, D. Vashaee, H. Guilbert, A. Pillitteri, M. S. Dresselhaus, G. Chen and Z. F. Ren, "Increased Phonon Scattering by Nanograins and Point Defects in Nanostructured Silicon with a Low Concentration of Germanium," Physical Review Letters, vol. 102, 2009.

[7] B. Yu, M. Zebarjadi, H. Wang, K. Lukas, H. Wang, D. Wang, C. Opeil, M. Dresselhaus, G. Chen and Z. Ren, "Enhancement of Thermoelectric Properties by Modulation-Doping in Silicon Germanium Alloy Nanocomposites.," Nano Letters, vol. 12, no. 4, p. 2077–2082, 2012.

[8] L. K. Eckler and D. M. Herlach, "Evidence for Transitions from Lateral to Continuous and to Rapid Growth in Ge-lat%Si Solid Solution.," Europhysics Letters, vol. 32, no. 3, pp. 223-227, 1995.

[9] R. P. Liu, T. Volkmann and D. M. Herlach, "Undercooling and solidification of Si by electromagnetic levitation," Acta Materialia, vol. 49, p. 439–444, 2001.

[10] C. Panofen and D. M. Herlach, "Rapid solidification of highly undercooled Si and Si–Co melts," Applied Physics Letters, vol. 88, 2006.

[11] P. Zhang, Z. Wang, H. Chen, H. Yu, L. Zhu and X. Jian, "Effect of Cooling Rate on Microstructural Homogeneity and Grain Size of n-Type Si-Ge Thermoelectric Alloy by Melt Spinning," Journal of Electronic Materials, vol. 39, no. 10, pp. 2251-2254, 2010.

[12] H. Nagai, Y. Nakata, H. Minagawa, K. Kamada, T. Tsurue, M. Sasamori and T. Okutani, "Synthesis of Si–Ge Alloy by Rapid Cooling in Short-Duration Microgravity," Japanese Journal of Applied Physics, vol. 41, pp. 749-753, 2002.

[13] C. Panofen and D. Herlach, "Solidification of highly undercooled Si and Si-Ge melts," Materials Science and Engineering A, Vols. 449-451, pp. 699-703, 2007.

[14] D. Herlach, D. Simons and P.-Y. Pichon, "Crystal growth kinetics in undercooled melts of pure Ge, Si and Ge-Si alloys," Philosophical Transactions A, vol. 376, no. 2113, 2018.

[15] O. Oloyede, T. D. Bigg, R. F. Cochrane and A. M. Mullis, "Microstructure evolution and mechanical properties of drop-tube processed, rapidly solidified grey cast iron," Materials Science & Engineering A, vol. 654, p. 143–150, 2016.

[16] N. Hussain, A. M. Mullis and J. S. Forrester, "Effect of cooling rate and chromium doping on the microstructure of Al-25 at.% Ni Raney type alloy," Journal of Alloys and Compounds, vol. 744, pp. 801-808, 2018.

[17] J. Schindelin, I. Arganda-Carreras, E. Frise, V. Kaynig, M. Longair, T. Pietzsch, S. Preibisch, C. Rueden, S. Saalfeld, B. Schmid, J.-Y. Tinevez, D. J. White, V. Hartenstein, K. Eliceiri, P. Tomancak and A. Cardona, "Fiji: an open-source platform for biological-image analysis," Nature Methods, vol. 9, p. 676–682, 2012.

[18] N. Wang and B.-B. Wei, "Droplet Undercooling During Containerless Processing in a Drop Tube," Chinese Physics Letters, vol. 21, no. 6, pp. 1120 - 1123, 2004.

List of Figures

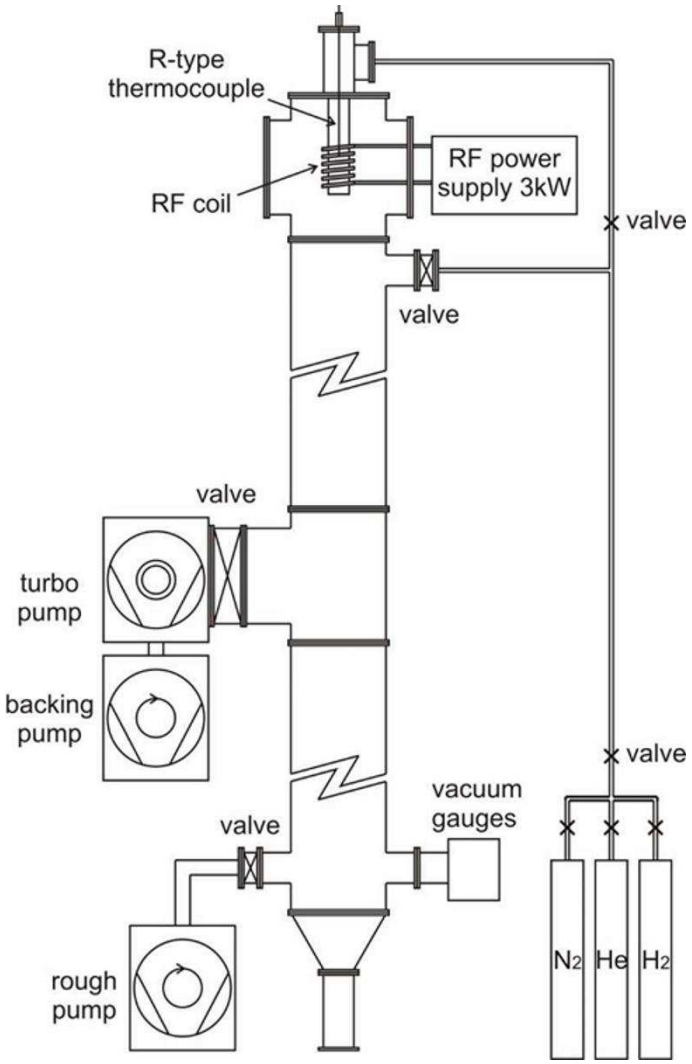

Figure 1: Schematic diagram of the drop-tube used to produce rapidly solidified powders.

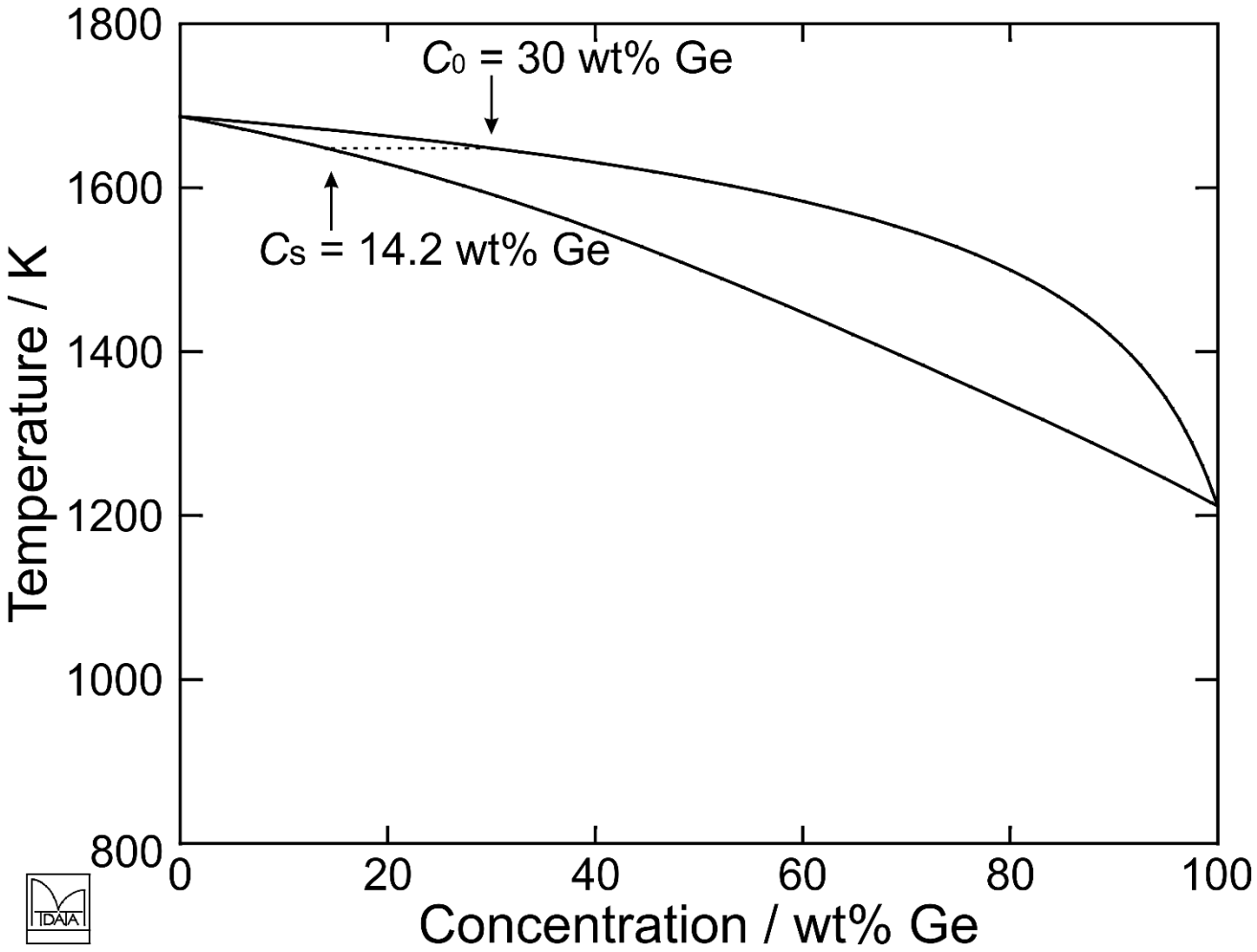

Figure 2: Calculated equilibrium phase diagram for the Si-Ge system.

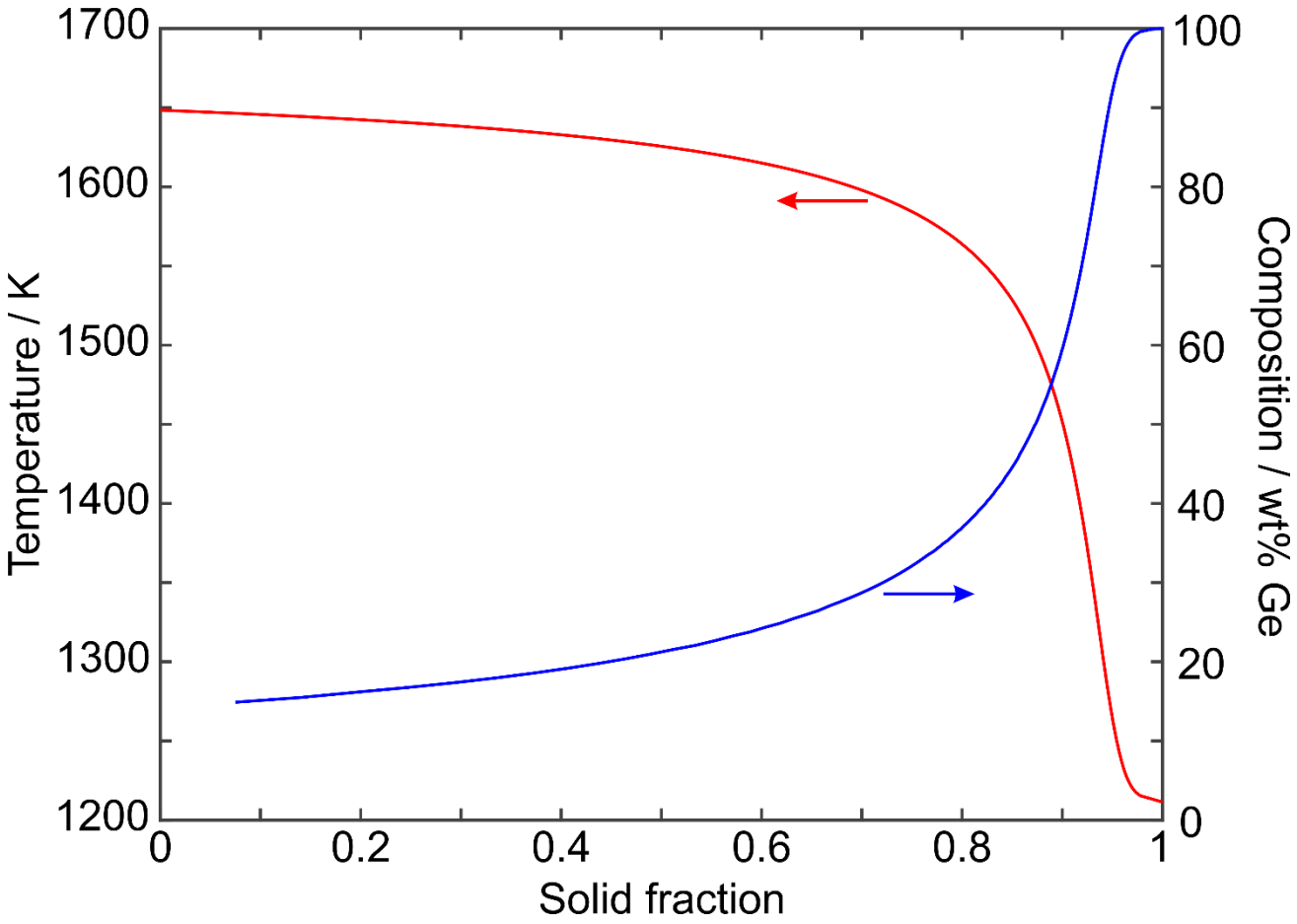

Figure 3: Scheil solidification calculation of the temperature and concentration of the solid formed at that temperature as a function of the solid fraction.

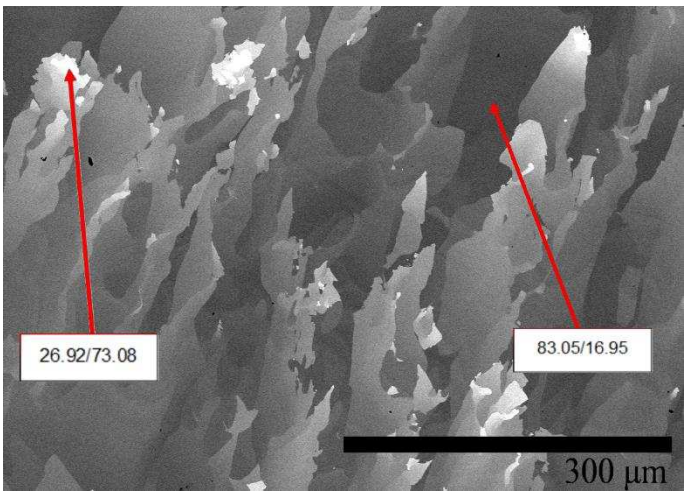

Figure 4: SEM backscattered micrograph and EDX point measurements in wt.% of starting material.

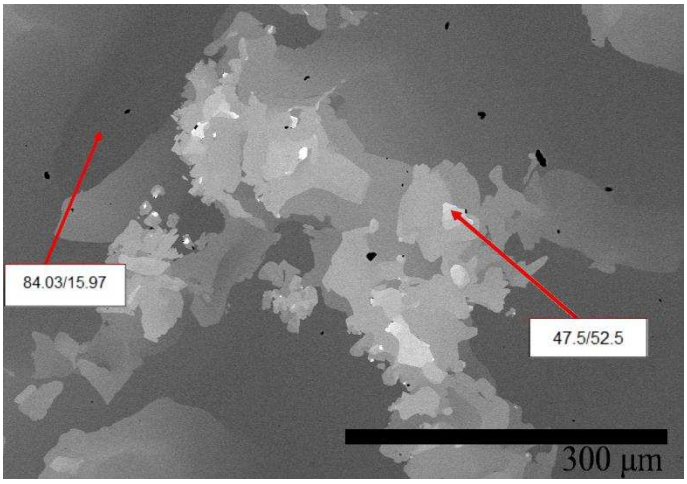

Figure 5: SEM backscattered micrograph and EDX point measurements in wt.% of the crucible residual sample.

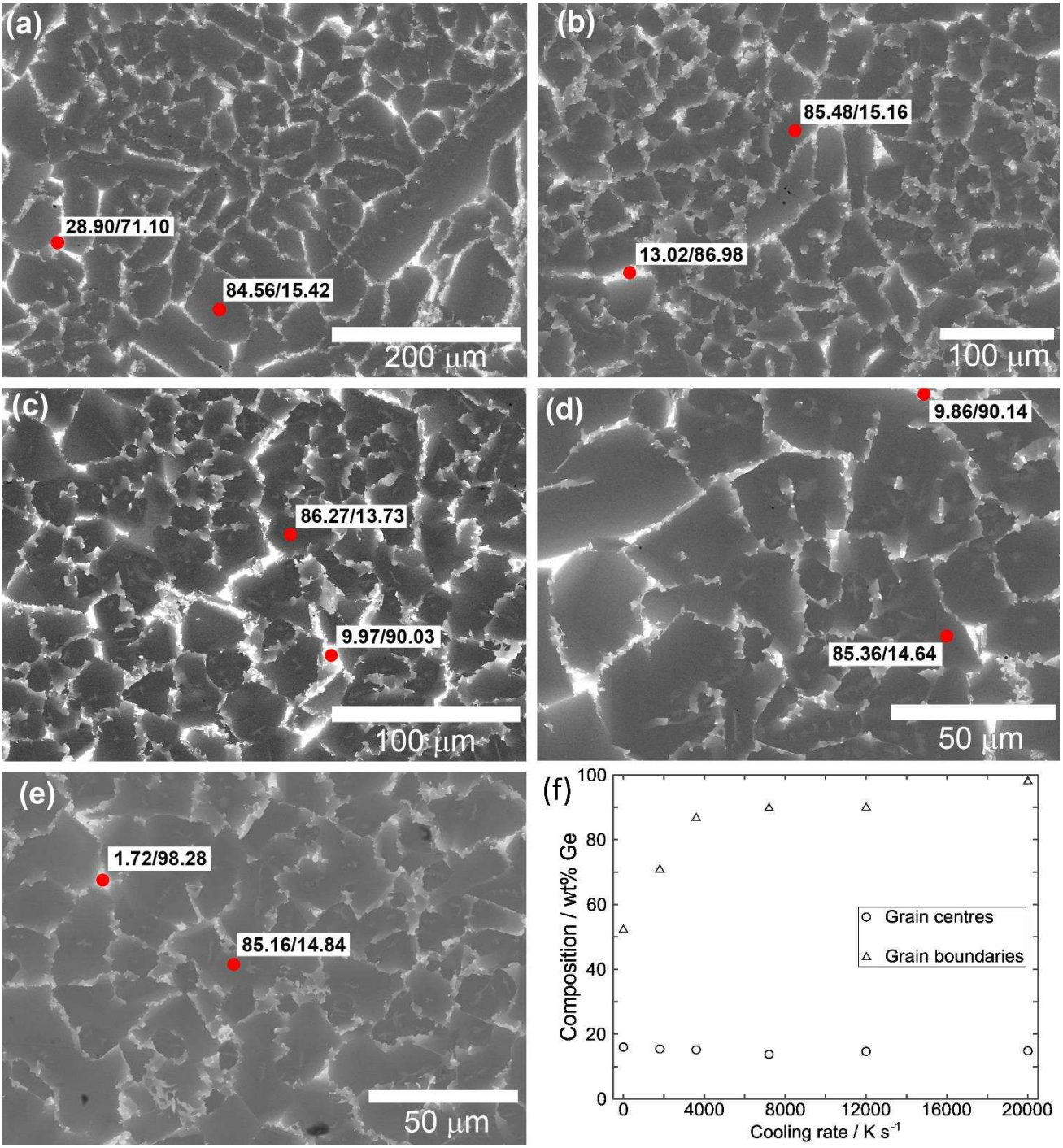

Figure 6: SEM backscattered micrographs and EDX point measurements in wt.% of rapidly solidified samples ranging from A) 850 µm < d, B) 500 µm < d < 850 µm, C) 300 µm < d < 500 µm, D) 212 µm < d < 300 µm and E) 150 µm < d < 212 µm.

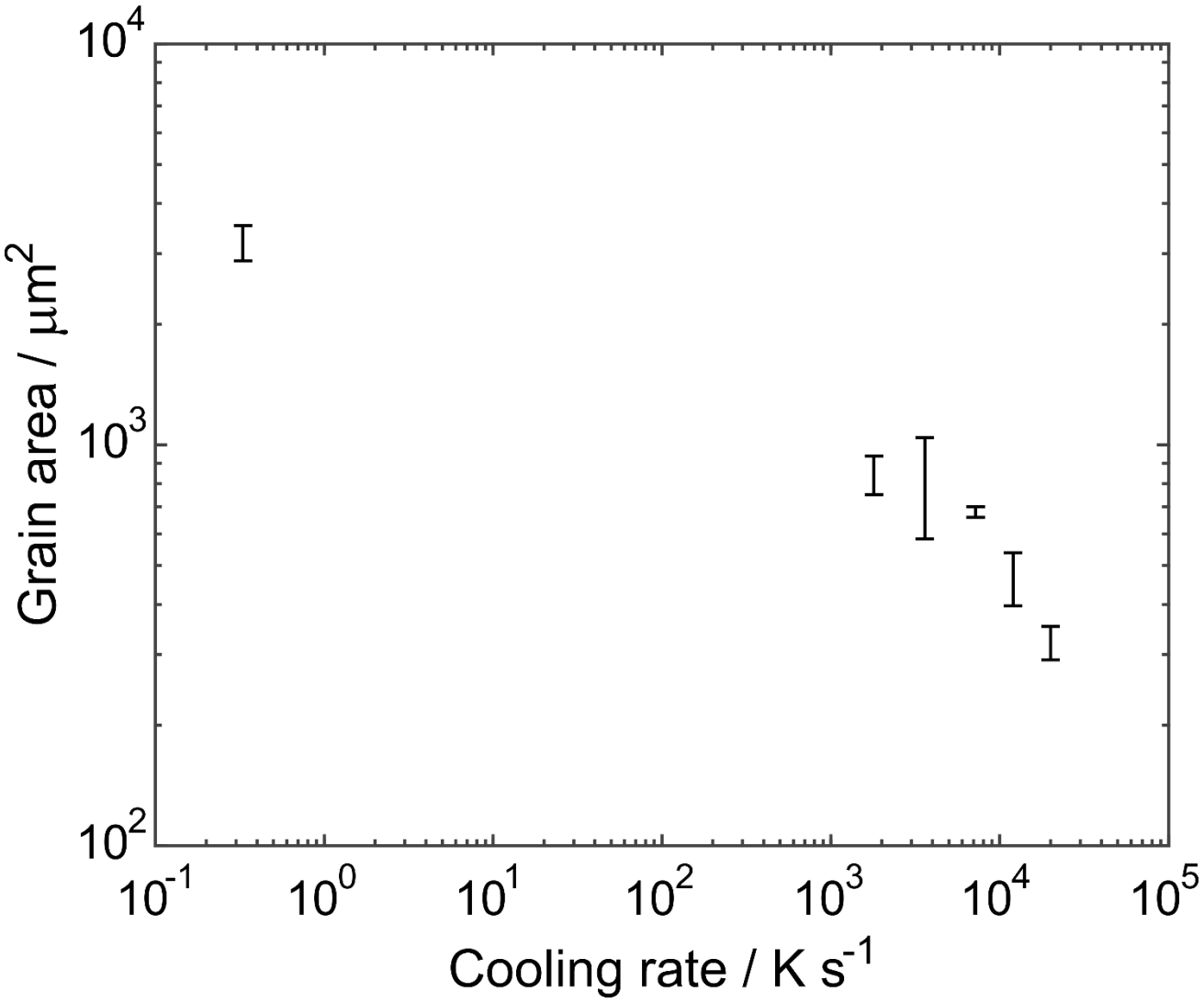

Figure 7: Average grain area of Si-rich regions as a function of cooling rate.

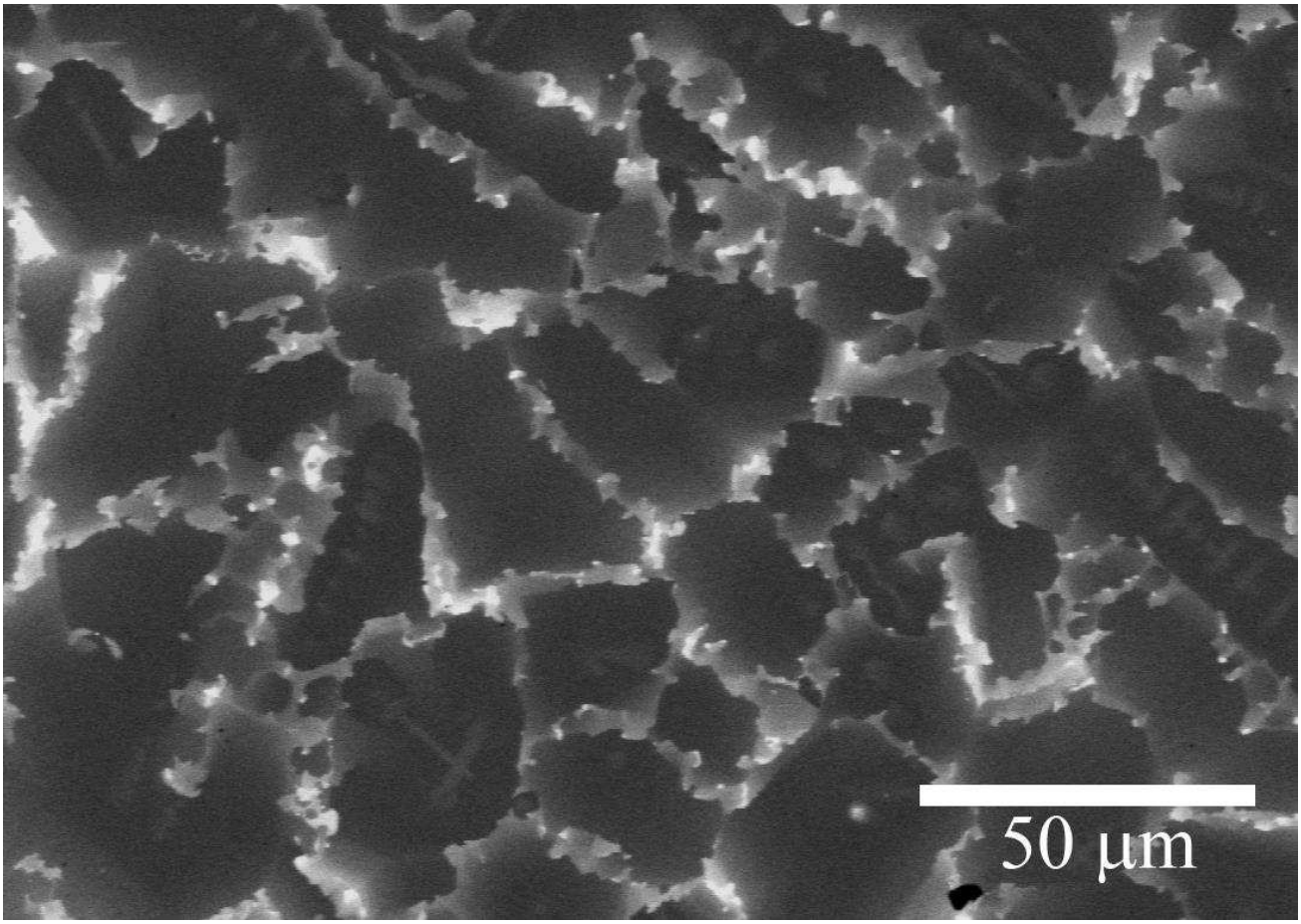

Figure 8: High magnification backscatter micrograph taken from the 300 – 500 μm sieve fraction showing the appearance of small distinct Ge-rich crystallites decorating the boundaries of the much larger Si-rich grains.

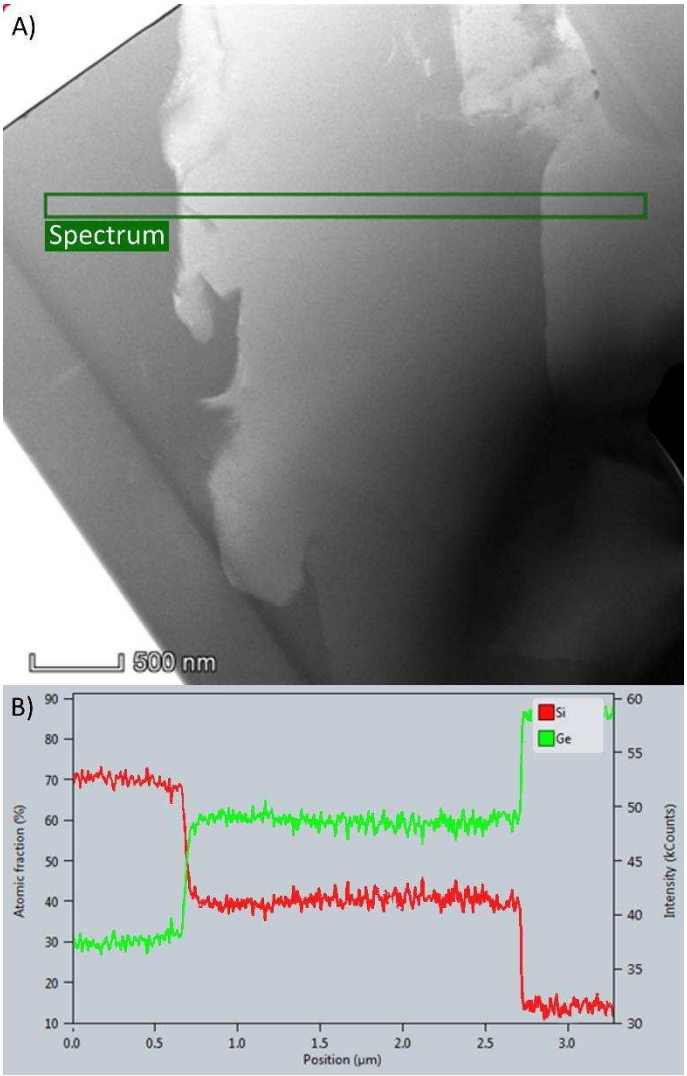

Figure 9: A) TEM brightfield image of SiGe showing Si-rich, Ge-rich and stoichiometric region. The Green rectangle illustrates the regions subject to TEM linescan. B) Elemental composition linescan obtained from green rectangle.

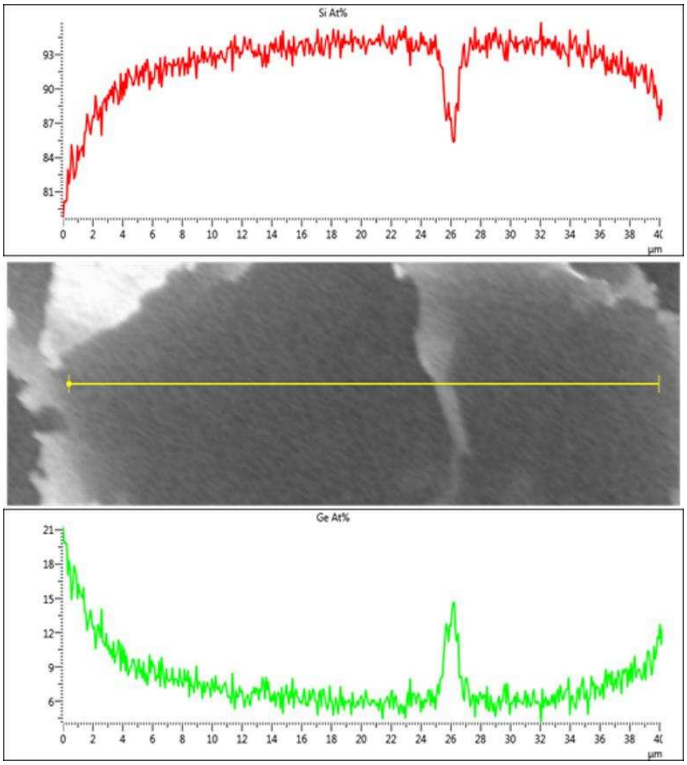

Figure 10: SEM EDX linescan conducted on an entire Si-rich grain illustrating the elemental composition from the centre of the grain to the grain boundary. For radial growth outwards from the grain centre this would be indicative of the concentration as growth proceeds.

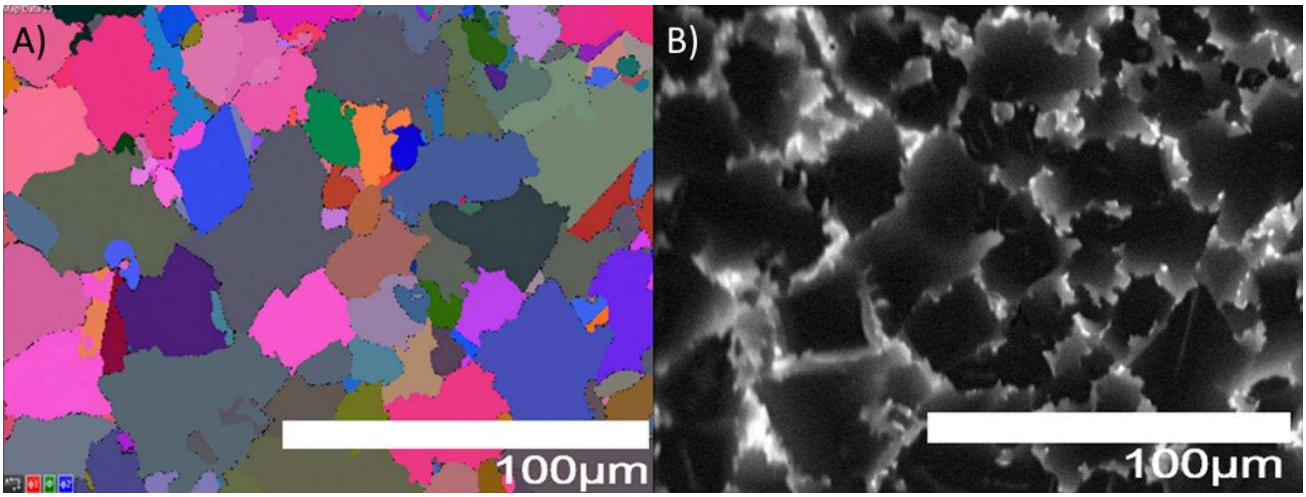

Figure 11: A) Euler (crystal orientation mismatch) map of SiGe grains in a rapidly solidified sample. B) SEM backscattered image to match Euler map showing Si-rich and Ge-rich regions.

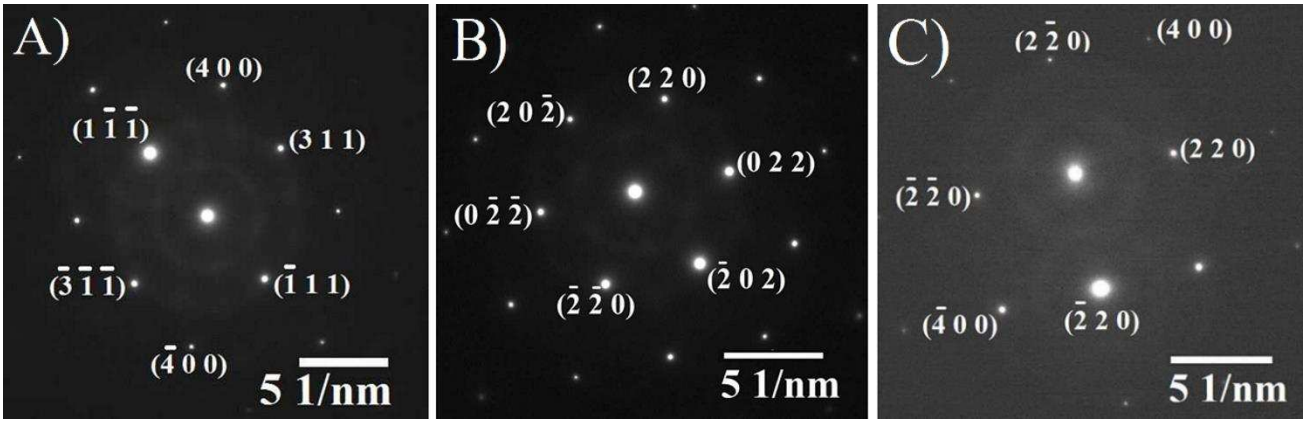

Figure 12: Selected area diffraction pattern of A) Ge-rich region, B) Intermediate region, and C) Si-rich region.